NANO LETTERS

pubs.acs.org/NanoLett

Letter

Design Principles for Fluorinated Interphase Evolution via Conversion-Type Alloying Processes for Anticorrosive Lithium Metal Anodes

Min-Ho Kim, Tae-Ung Wi, Jeongwoo Seo, Ahreum Choi, Sangho Ko, Juyoung Kim, Ukhyun Jung, Myeong Seon Kim, Changhyun Park, Sunghwan Jin, and Hyun-Wook Lee*

Cite This: *Nano Lett.* 2023, 23, 3582−3591

Read Online

ACCESS | Metrics & More | Article Recommendations | Supporting Information

ABSTRACT: Over the past decade, lithium metal has been considered the most attractive anode material for high-energy-density batteries. However, its practical application has been hindered by its high reactivity with organic electrolytes and uncontrolled dendritic growth, resulting in poor Coulombic efficiency and cycle life. In this paper, we propose a design strategy for interface engineering using a conversion-type reaction of metal fluorides to evolve a LiF passivation layer and Li-M alloy. Particularly, we propose a LiF-modified Li-Mg-C electrode, which demonstrates stable long-term cycling for over 2000 h in common organic electrolytes with fluoroethylene carbonate (FEC) additives and over 700 h even without additives, suppressing unwanted side reactions and Li dendritic growth. With the help of phase diagrams, we found that solid-solution-based alloying not only facilitates the spontaneous evolution of a LiF layer and bulk alloy but also enables reversible Li plating/stripping inward to the bulk, compared with intermetallic compounds with finite Li solubility.

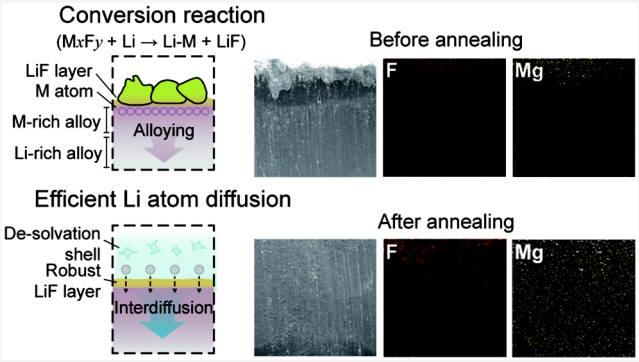

KEYWORDS: *lithium metal batteries, binary phase diagram, conversion reaction, alloying type, fluorinated interphase*

Developing high-energy-density rechargeable batteries is crucial for achieving next-generation vehicles and aircraft.[1] Over the past decade, lithium metal has emerged as one of the most promising anode materials for high-energy-density batteries due to its highest specific capacity (3860 mAh g^{-1}) and lowest reduction potential (−3.040 V versus the standard hydrogen electrode).[2−4] Despite its merits, dendritic Li growth and its high reactivity with organic electrolytes have impeded its practical applications, resulting in low Coulombic efficiencies (CE), poor cyclability, and safety concerns.[5,6]

For the aforementioned challenges associated with Li metal anodes, interface engineering is a critical requirement to mitigate persistent side reactions between fresh Li and electrolytes.[7−10] Since the solid electrolyte interphase (SEI) layer formed at the electrode/electrolyte interface functions as a versatile functional film during battery operation, researchers have focused on designing a robust and chemically stable SEI layer, which plays a crucial role in reversible Li plating/stripping behaviors.[11−15] Although early studies on Li metal used ether-based electrolytes[16] and highly concentrated electrolytes[17] to yield meaningful outcomes in terms of CE and cyclability, concerns for its feasibility have been still raised due to its incompatibility with 4 V class cathode materials and high costs.[18]

To overcome these shortcomings, researchers have had great interest in inorganic-rich SEI layers, particularly fluorinated SEI layers with high LiF contents as crucial passivation films for stable Li metal systems.[19−21] During battery operation, the fluorinated SEI layer is typically formed by the decomposition of F-incorporated solvents such as fluoroethylene carbonate (FEC)[22] or F-rich Li salts,[23] including lithium bis-trifluoromethanesulfonimide (LITFSI), lithium bis(fluorosulfonyl)-imide (LIFSI), and lithium difluoro(oxalate)borate (LiDFOB). Theoretically, the lowest unoccupied molecular orbital (LUMO) of F-incorporated species is lower than that of common organic solvents because of the strong electron-withdrawing property of F-containing functional groups.[19] This means that F-incorporated species can preferentially decompose into LiF species before other solvents to protect the Li metal surface from reactive species.

Received: February 27, 2023
Revised: April 4, 2023
Published: April 7, 2023

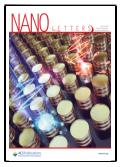

ACS Publications

© 2023 American Chemical Society

https://doi.org/10.1021/acs.nanolett.3c00764
Nano Lett. 2023, 23, 3582−3591

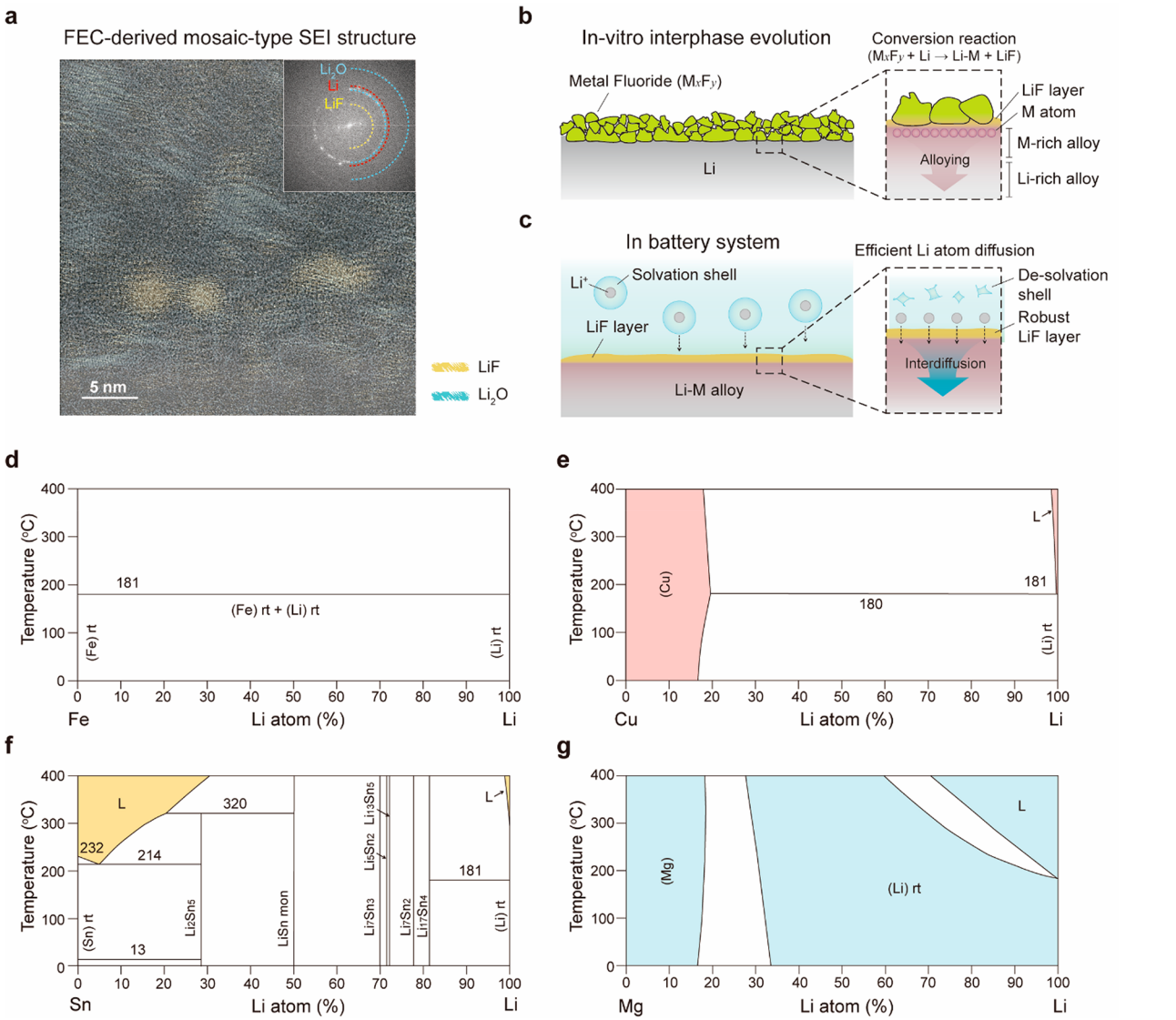

Figure 1. Characterization of the SEI layer formed on Li deposits and interface engineering. (a) Cryogenic TEM image of the SEI layer formed on deposited Li in organic electrolytes with FEC additives. The inset demonstrates the corresponding SAED pattern. (b) Schematic illustration of *in vitro* interphase evolution employing the conversion reaction of metal fluorides, M_xF_y + Li → Li-M + LiF. (c) Schematic illustration of Li plating/stripping of Li-M alloy with the LiF outermost layer. After desolvating solvents, Li ions efficiently diffuse in Li-M alloy, as the LiF layer prevents side reactions between Li-M alloy and organic electrolytes. (d−g) Binary phase diagram of Li-Fe, Li-Cu, Li-Sn, and Li-Mg. Phase diagrams of Li-Fe and Li-Cu show that Li does not react with Fe, but a small quantity of Li can dissolve into Cu within the narrow soluble region (red). Meanwhile, in the case of Li-Sn and Li-Mg, their alloy phases can be formed differently. The Li-Sn phase diagram exhibits many solid phases with definite stoichiometry, known as an intermetallic alloy system. It has an ordered uniform structure, but phase precipitation may occur in the off-stoichiometric state. However, the Li-Mg phase diagram shows two large solubility zones (Mg-rich and Li-rich zones), called a solid-solution system. It has a nonuniform structure, but no solubility limits, which could be beneficial for persistent Li plating.

At the same time, the emergence of *cryogenic* transmission electron microscopy (cryo-TEM) technology also has enormously contributed to the recent advances of the SEI layer by allowing the characterization of the structure at the atomic level.[24−26] Not so long ago, researchers believed that the LiF composites are uniformly distributed along the Li surface in the form of a thin film. However, contrary to our expectations, cryo-TEM images of Li deposited in organic electrolyte systems with FEC additives demonstrated that the inorganic-rich SEI layer on the Li surface primarily consists of Li_2O components instead of LiF and retains an inhomogeneous mosaic-type structure, which is consistent with our observation (Figure 1a). Therefore, the previously proposed methods involving the evolution of a dense and uniform inorganic-rich SEI layer with high LiF content require further validation for their efficacy.

In this study, we propose a design approach in which the simultaneous *in vitro* interphase evolution of robust LiF inorganic compounds and lithium alloy (Li-M) enhances chemical stability with carbonate-based organic electrolytes through pretreatment of metal fluoride material (M_xF_y) onto Li metal electrodes at a relatively low annealing temperature of 300 °C. Particularly, we emphasize the importance of the presence of the Li-M alloy phase to facilitate a uniform interphase layer and promote facile Li diffusion. We experimentally analyzed that metal fluoride (MF_x) decomposes into metal (M) nanoparticles and LiF when it reacts with Li.[27−29] We discovered that the metal-forming alloy phase with

https://doi.org/10.1021/acs.nanolett.3c00764
Nano Lett. 2023, 23, 3582−3591

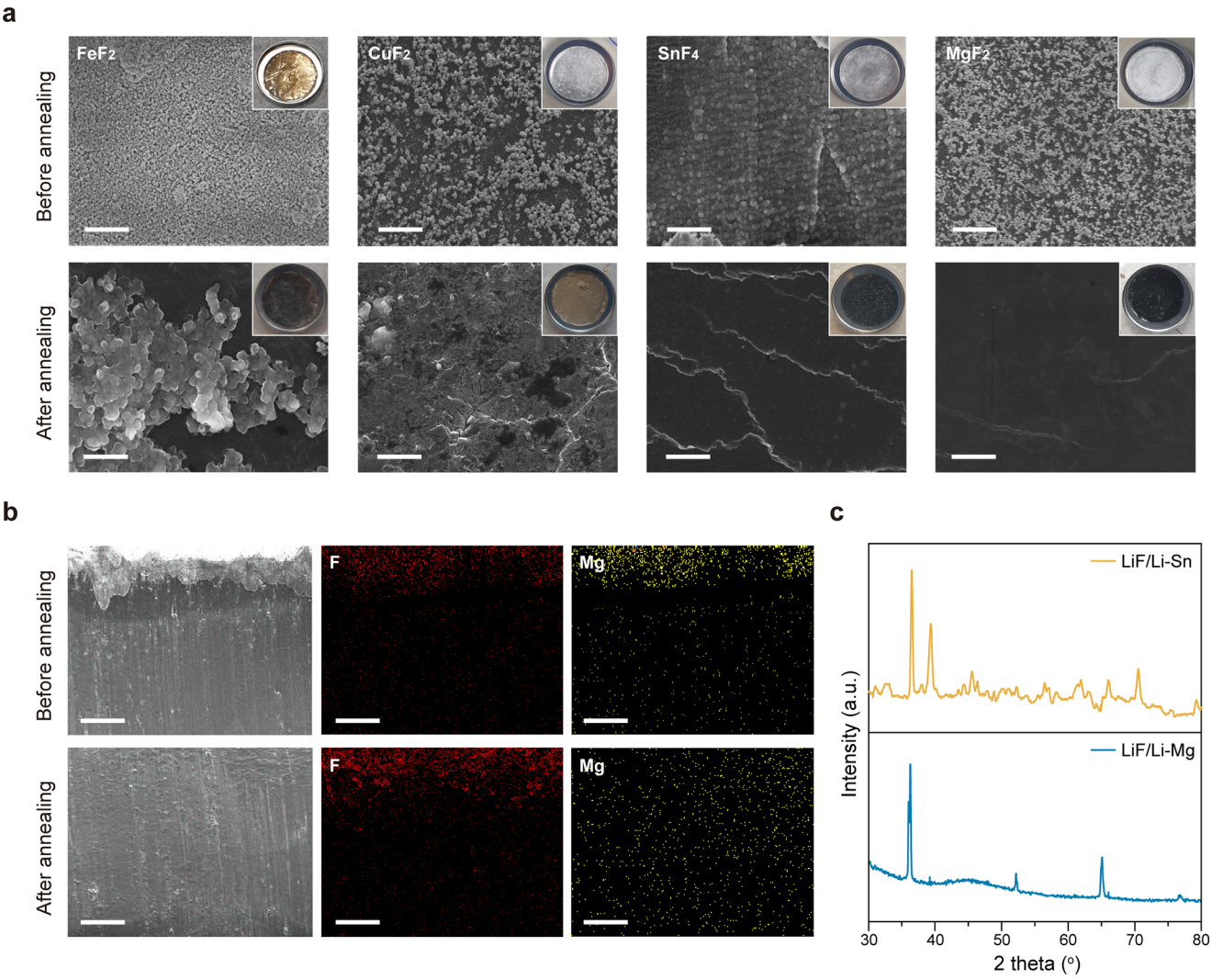

Figure 2. Morphology studies of LiF/Li-M alloys (M = Fe, Cu, Sn, and Mg). (a) SEM images of metal fluoride (M_xF_y) treated Li electrodes before and after annealing. The insets depict digital images of the electrodes. The scale bar is 2 μm. (b) Cross-sectional SEM and corresponding EDS images for the LiF/Li-Mg electrodes. The scale bar is 10 μm. (c) XRD data of LiF/Li-Sn and LiF/Li-Mg electrodes, showing a multiphase structure and a single-phase structure, respectively.

Li guides a uniform LiF interphase layer and homogeneous bulk Li-M alloy (Figure 1b). Furthermore, we showed that this interface-engineered Li-M alloy enables stable Li plating/stripping through uniform atomic diffusion within the alloy phase, even in organic electrolytes without FEC additives (Figure 1c). We believe that this finding offers a scientific rationale for the phase-diagram-determined interface engineering of Li metal and a guideline for the rational selection of pretreatment materials.

We investigated four metal fluoride candidates composed of metal elements showing different types of Li-M binary phase diagrams: FeF_2, CuF_2, SnF_4, and MgF_2. Figure 1d−g illustrates each phase diagram of Li-Fe, Li-Cu, Li-Sn, and Li-Mg, respectively, demonstrating different characteristics. First, Fe does not form an alloy phase with Li at any composition (Figure 1d). Second, Cu, which is commonly used as a current collector in battery anodes and anode-free batteries,[30] has a limited solubility zone with Li in the Cu-rich region at room temperature (Figure 1e). However, its low solubility and significant lattice mismatch between Li-Cu and Li would guide Li deposition (or Li-Cu alloy precipitation) rather than the formation of a homogeneous alloy phase. Third, Sn, which is a representative alloying material to aid facile Li and Na deposition,[31] forms several alloy phases across the entire composition ratio, which are known as intermetallic compounds[32,33] (Figure 1f). Generally, intermetallic compounds have uniform and ordered structures in a finite stoichiometric composition ratio. However, its off-stoichiometric nature can drive phase precipitation/phase separation depending on the compositions. Furthermore, according to a previous report,[34] its nonuniform phase transition also hinders efficient Li plating/stripping, which may be unsuitable for Li systems, case by case. Lastly, Mg forms two solid-solution phases (Mg-rich α-phase (space group: $P6_3/mmc$) and Li-rich β-phase (space group: $Im\bar{3}m$)) with no solubility limit[35,36] (Figure 1g). Li atoms can diffuse in/out of the bulk without a phase transformation within the solid-solution phase, guiding the spontaneous formation of the alloy phase throughout both synthesis and battery operation. Therefore, we conceptually discovered that Fe and Cu are inappropriate for Li metal surface engineering. However, Sn and Mg can form a desirable Li/electrolyte interphase layer. Nevertheless, Li-Sn intermetal-

https://doi.org/10.1021/acs.nanolett.3c00764
Nano Lett. 2023, 23, 3582−3591

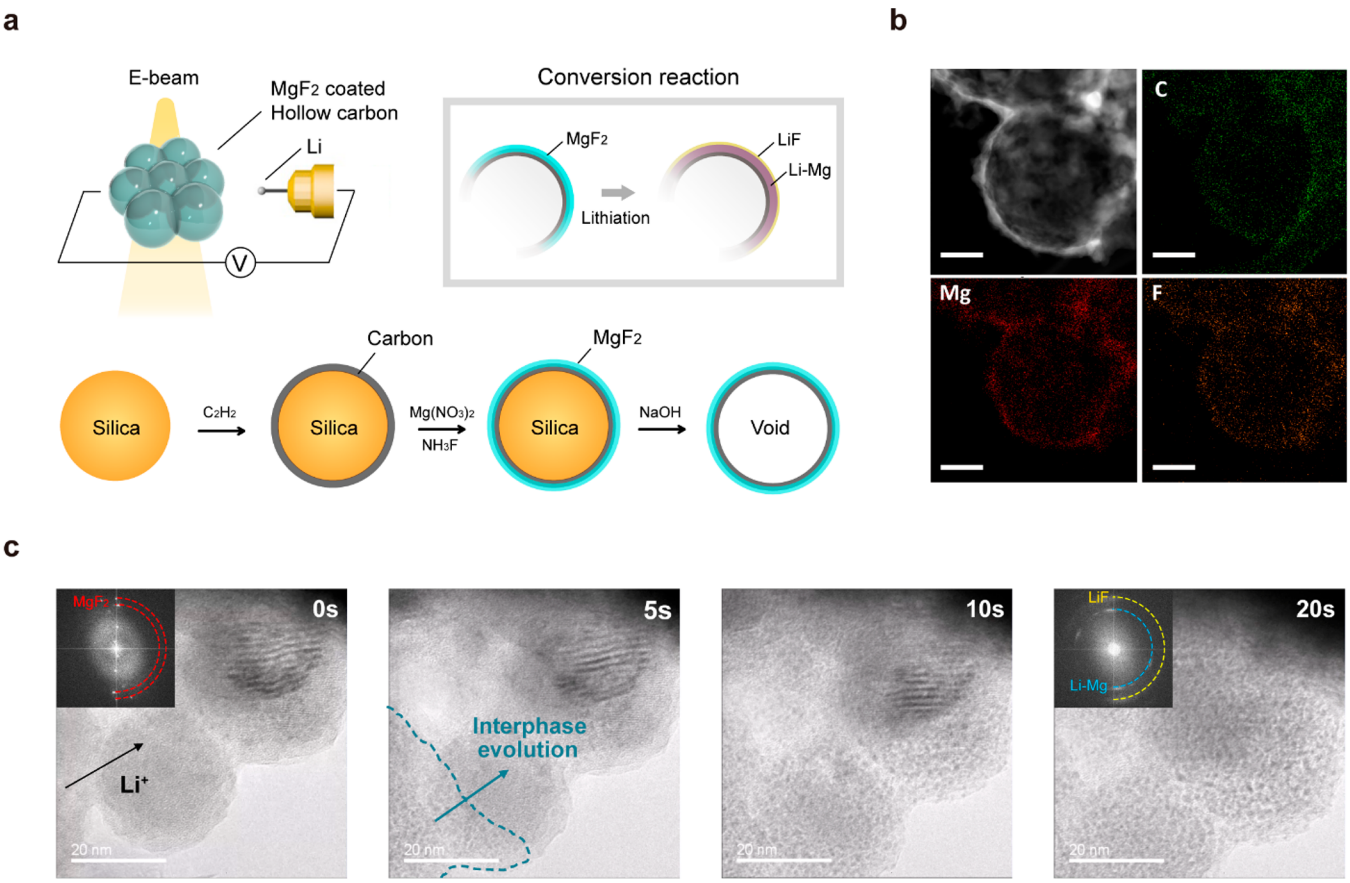

Figure 3. *In situ* observation of interphase evolution during the conversion reaction of MgF_2. (a) Schematic illustrations of MgF_2/C hollow sphere design. (b) High-resolution TEM image of an MgF_2/C hollow sphere and corresponding EDS mapping images. The scale bar is 5 μm. (c) TEM snapshots of the interphase evolution during the conversion reaction with Li under electric bias.

lic compounds might cause heterogeneous Li plating accompanied by multiple phase transitions/precipitations during the Li plating/stripping. Here we chose Mg as the most suitable alloying candidate because of its infinite Li solubility and negligible phase transformation via the solid-solution reaction. According to previous reports,[35−37] Li-Mg alloy facilitates uniform Li alloying/plating due to its very high lithium diffusion coefficient of $D \approx 10^{-7}$ cm^2 s^{-1}, indicating its promise as a long-term alternative to pure Li metal anodes. Similarly, MgF_2 would be the most attractive material for designing the fluorinated SEI layer on Li-M alloys through a conversion reaction.

We compared the surface morphologies of the aforementioned metal fluoride treated Li-M alloys to experimentally prove the hypothesis (Figure 2a). As shown in scanning electron microscopy (SEM) images, metal fluoride nanoparticles cover the entire Li surface in common before annealing. However, the annealed electrodes retain different surface morphologies. In the case of electrodes including Fe with no alloy phase with Li, Fe nanoparticles exist in the agglomerated state, as proved through XRD (Figure S1). In the case of Cu with a low solubility of Li, however, its nonhomogeneous surface was observed instead of residual nanoparticles. We concluded that the incomplete reaction between Li and Cu causes the phase separation of Cu, Li, and Li-Cu.

In contrast to FeF_2 and CuF_2 demonstrating imperfect interface engineering, the use of SnF_4 and MgF_2 showed clear interphase evolution. As a result, we discovered that the existence of the alloy phase over the entire composition ratio of Li and metal facilitates spontaneous interface engineering during annealing when these metal fluorides are used. In a previous report,[27] it was confirmed through DFT computation that the high surface and interfacial energy of LiF thermodynamically prevents its penetration into bulk Li (or Li-Al), remaining near the surface in the form of a LiF layer. Likewise, we thought that while Sn or Mg atoms diffuse into bulk Li melts to form the alloy phase during annealing, the LiF interphase layer would evolve at the top surface of the electrode. Indeed, the cross-sectional SEM images energy dispersive spectroscopy (EDS) demonstrate that F and Mg (or Sn) are distributed separately within the annealed electrode, compared to the dried electrodes where F and Mg (or Sn) are evenly distributed on the electrode surface (Figure 2b and Figure S3). Thus, an LiF interphase layer was successfully achieved through a conversion reaction between Li and MgF_2 (or SnF_2).

In spite of their morphological similarity, there exists a large gap between MgF_2- and SnF_4-treated electrodes in XRD results (Figure 3c). Although both appear to have smooth and uniform surfaces on SEM images, the SnF_4-treated sample has a multiphase structure composed of various Li-Sn compositions (Figure S4). In contrast, the MgF_2-treated sample consists of a single Li-rich alloy phase (Figure S5). That is why we chose MgF_2 as a target material for achieving interface-reinforced uniform Li electrodes in this study.

https://doi.org/10.1021/acs.nanolett.3c00764
Nano Lett. 2023, 23, 3582−3591

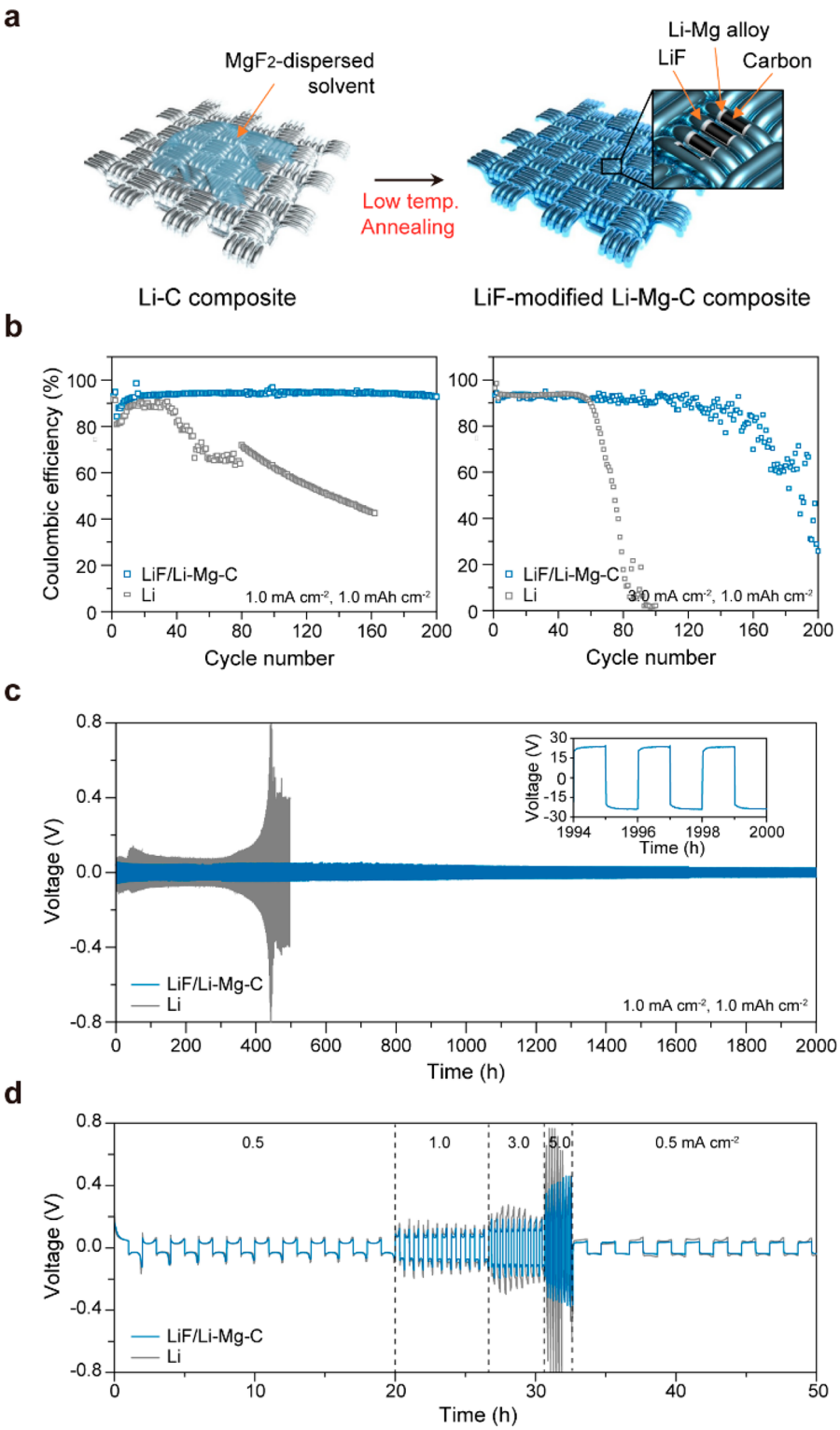

Figure 4. Electrochemical characterization of LiF/Li-Mg-C electrodes in an organic electrolyte system with FEC additive. (a) Schematic illustration of LiF/Li-Mg-C electrode design through the conversion reaction of MgF_2 with Li-C composites. (b) Asymmetric cell evaluations measured at a current density of 1.0 mA cm^{-2} (left) and 3.0 mA cm^{-2} (right) with a fixed areal capacity of 1.0 mAh cm^{-2}. (c) Galvanostatic voltage profiles of symmetric cells measured at a current density of 1.0 mA cm^{-2} with an areal capacity of 1.0 mAh cm^{-2}. (d) Rate capability at current densities of 0.5, 1.0, 3.0, and 5.0 mA cm^{-2} for every 10 cycles. All the cell evaluations were measured in organic electrolytes, 1.3 M $LiPF_6$ in EC/DEC = 3:7 + 10 wt % FEC.

To demonstrate the reaction mechanism of MgF_2 with Li into LiF and Li-Mg alloy, we conducted an *in situ* TEM analysis employing a dual-probe biasing TEM holder (Figure 3 and Video S1). For the convenience of TEM observation, we synthesized MgF_2-anchored carbon nanocapsules[38] that are translucent to an electron beam, as illustrated in Figure 3a. The synthesized nanocapsules were characterized by EDS elemental mapping (Figure 3b), which confirmed that the MgF_2

https://doi.org/10.1021/acs.nanolett.3c00764
Nano Lett. 2023, 23, 3582−3591

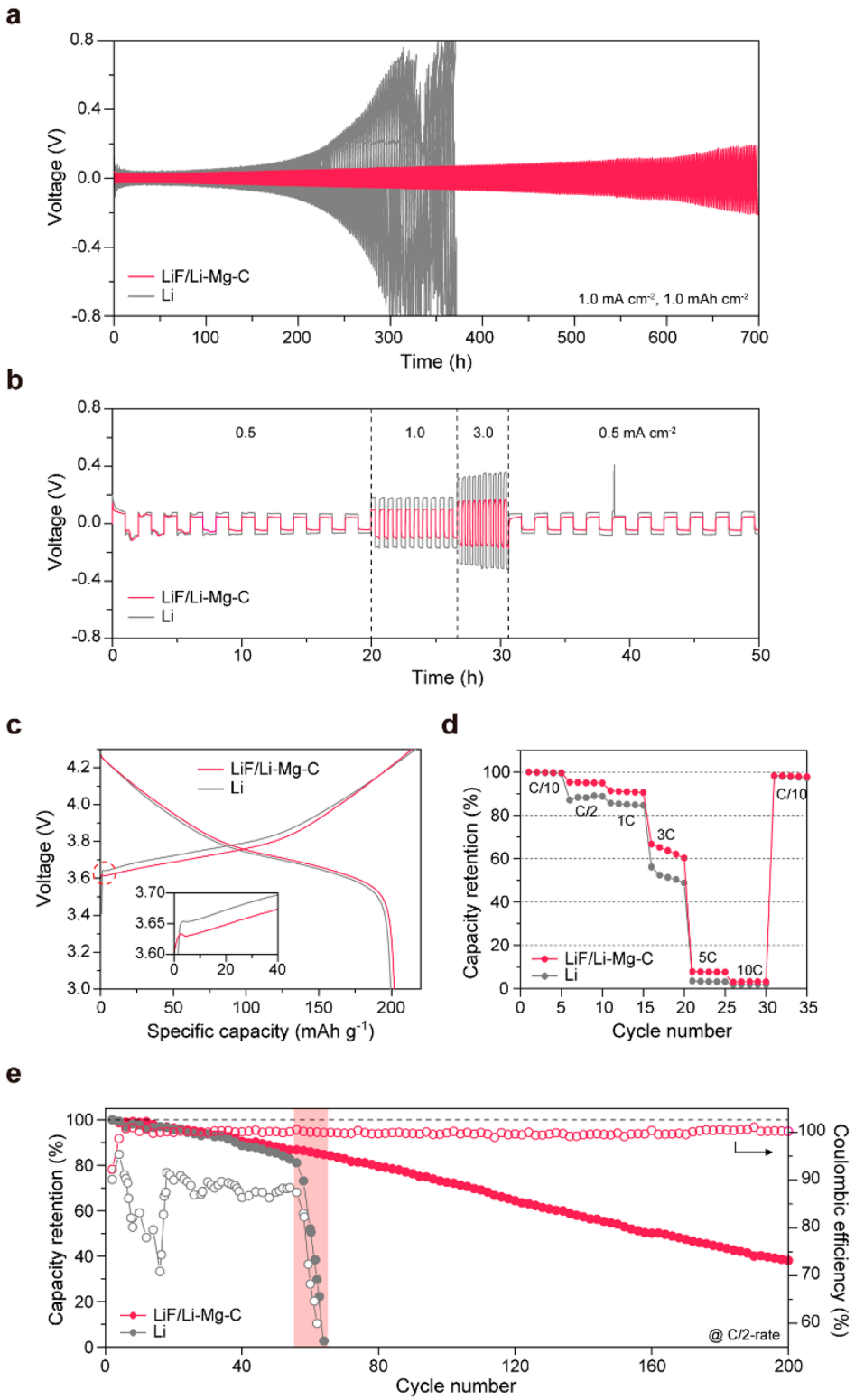

Figure 5. Electrochemical characterization of LiF/Li-Mg-C electrodes in an organic electrolyte system with no additive. (a) Galvanostatic voltage profiles of symmetric cells measured at a current density of 1.0 mA cm^{-2} with an areal capacity of 1.0 mAh cm^{-2}. (b) Rate capability at current densities of 0.5, 1.0, and 3.0 mA cm^{-2} for every 10 cycles. (c−e) Full-cell evaluations of Li|NCM and LiF/Li-Mg-C|NCM. (c) Corresponding voltage profiles at the 1st cycle. The inset shows a voltage "bump" at the beginning of charging. (d) Rate capability at the various C-rates (C/10, C/2, 1C, 3C, 5C, and 10C). (e) Cycle retention of the full cells at C/2-rate, demonstrating the superiority of LiF/Li-Mg-C electrodes. All of the cell evaluations were measured in organic electrolytes, 1.3 M $LiPF_6$ in ECEC/DMC = 3:4:3.

nanoseeds successfully adhere to the hollow carbon spheres. As soon as current was applied to deposit Li metal, numerous Li-Mg nanograins were rapidly formed within the LiF, which is typical conversion reaction behavior[39] (Figure 3c). Electron diffraction patterns (the insets in Figure 3c) exhibit that MgF_2 disappeared and Li-Mg and LiF appeared during the interphase

https://doi.org/10.1021/acs.nanolett.3c00764
Nano Lett. 2023, 23, 3582−3591

evolution. Particularly, after the initial phase evolution occurred from the interface between Li and MgF_2, the reaction fronts quickly propagate across the interparticle boundary, indicating that the Li diffusion/reaction kinetics within LiF/Li-Mg composites is considerably fast.

The MgF_2-treated Li electrodes were subjected to electrochemical evaluation using coin-type asymmetric and symmetric cells. Specifically, we treated MgF_2 onto Li-infiltrated carbon cloth (Li-C composite) instead of Li metal foil (Figure 4a). In a previous report,[40] we demonstrated that the carbon cloth serves as a scaffold to keep the Li electrode morphology constant and suppresses dendritic Li growth by homogenizing Li ionic flux. Additionally, this Li-C composite allows easy handling of the electrode above the melting temperature of Li (180.5 °C). LiF-modified Li-Mg-C composites (hereafter denoted as LiF/Li-Mg-C composite) was successfully obtained through the fabrication process shown in Figure S6. The surface morphology of the as-synthesized final composite was imaged using SEM (Figure S7).

First, we assembled Cu|LiF/Li-Mg-C asymmetric cells using carbonate-based organic electrolytes with FEC additives (1.3 M $LiPF_6$ in EC/DEC = 3:7 + 10 wt % FEC) (Figure 4b). LiF/Li-Mg-C demonstrated an almost constant Coulombic efficiency (CE) of 94.2% over 200 cycles while operating the cells at 1.0 mA cm^{-2} with a fixed areal capacity of 1.0 mAh cm^{-2}. However, Li metal showed considerable cell decay, which might be due to a side reaction with the electrolytes and the formation of dead Li, despite the presence of FEC additives. Furthermore, when cycled at 3.0 mA cm^{-2}, LiF/Li-Mg-C maintained its CE of 92.7% for 100 cycles, while Li metal demonstrated a rapidly decreasing CE just after 60 cycles. These findings show that the synergetic effect of the LiF outermost layer and Li-Mg alloy enhances homogeneous Li alloying (or deposition) by inhibiting its side reaction and dead Li formation, eventually extending its cell lifetime. Additionally, we observed similar benefits in symmetric cells, which exhibited a sharp contrast to Li symmetric cells (Figure 4c). At a current density of 1.0 mA cm^{-2} with an areal capacity of 1.0 mAh cm^{-2}, LiF/Li-Mg-C composites demonstrated stable long-term cycling over 2000 cycles, while Li metals demonstrated rapidly increased overpotential just after 300 cycles. Even after 2000 cycles, the composites demonstrated a low overpotential of 20 mV (the inset of Figure 4c). This indicates that the Li plating/stripping of LiF/Li-Mg-C composites operated stably without thick insulating interphase layer formation due to persistent electrolyte decomposition and dead Li, as proved through *ex situ* SEM images after cycling (Figure S8). Although cycled LiF/Li-Mg-C exhibits a rugged surface, its morphology is still far from that of typical dendritic Li, demonstrating that spontaneous Li diffusion inside the Li-Mg bulk through a solid-solution effectively suppresses dendritic Li. Furthermore, these low overpotentials benefit rate properties at various current densities (Figure 4d). When cells were cycled at current densities of 0.5, 1.0, 3.0, and 5.0 mA cm^{-2} every 10 cycles, the overpotentials of LiF/Li-Mg-C composites were 50, 85, 122, and 398 mV, respectively, which is significantly better than those of the Li metals that showed overpotentials of 63, 109, 165, and 670 mV, respectively. This implies that the interphase kinetics of the composites are significantly much better than those of Li metals, facilitating Li plating/stripping even under high current densities.

To investigate the impact of the preformed interphase layer on Li metal, we cycled the symmetrical cells using organic electrolytes without additives, which represents a harsh condition for Li metal batteries. Without electrolyte additives forming the passivation layer during the cycle, Li corrosion and side reactions with organic electrolytes can be significantly accelerated. Indeed, in the symmetric cell evaluation at 1.0 mA cm^{-2} (1.0 mAh cm^{-2}), Li metal shows sharply increased overpotentials after 200 h with significantly reduced cell lifetime (Figure 5a). In stark contrast, LiF/Li-Mg-C composites exhibited comparatively stable cycling over 700 h, except for the gradual increase in cell overpotential of 0.13 mV per cycle. This indicates that the preformed LiF layer and Li-Mg alloy successfully mitigate the interphase reaction with electrolyte and nonuniform Li growth. Similarly, its merit was also identified through the rate performance (Figure 5b). When the cell was operated at 0.5, 1.0, and 3.0 mA cm^{-2}, the cell overpotentials of the composite were 48.9, 96.5, and 162.9 mV, respectively, compared with those of Li metal, which were 75.5, 174.2, and 343.4 mV, respectively, demonstrating the superior interface stability and kinetics during Li plating/stripping.

For a more in-depth investigation, we paired the LiF/Li-Mg-C composite with commercial NCM811 cathodes to create a full cell in the same organic electrolytes with no additives. First, we compared the voltage profiles of each NCM811 cell with a loading density of 1.5 mAh cm^{-2} for the first cycle at a C/10-rate (Figure 5c). During the initial charging stage, the Li|NCM811 cell demonstrated a higher "potential hump" (indicated by a red dotted circle) corresponding to around 3.65 V than the LiF/Li-Mg-C|NCM811 cell, as illustrated in the inset of Figure 5c, which is consistent with the cell data provided so far. Such a hump could result from the hysteretic behaviors of cathodes and metal anodes. In turn, this indicates that LiF/Li-Mg-C electrodes effectively reduce cell overpotentials. Additionally, each initial CE (ICE) was 95.3% for LiF/Li-Mg-C|NCM811 and 94.5% for Li|NCM811, indicating the enhanced electrochemical reversibility of the composite. Similar to the cell data provided above, the full cell employing the composite also demonstrated significantly enhanced rate properties (Figure 5d), showing 63.5% for LiF/Li-Mg-C and 51.7% for Li at the 3C-rate. The outstanding electrochemical performance of the LiF/Li-Mg-C composite enables successful full-cell cycling performance at the C/2-rate (0.75 mA cm^{-2}) in a common organic electrolyte without additives (Figure 5e). In contrast to Li metal showing rapid capacity decay in just 60 cycles, the composites show an average CE of 99.58%. Its relatively high CE indicates that its gradual decrease in cell capacity may be caused by the degradation of NCM811 particles such as Ni dissolution, rather than LiF/Li-Mg-C composites.

To further investigate the synergetic effect of LiF and Li-Mg alloy, we performed electrochemical impedance spectroscopy (EIS) and air stability tests (Figures S9−S11). As shown in Figure S9, interfacial impedances of both electrodes after the initial cycle exhibit a slight difference (∼39 Ω for Li and ∼34 Ω for LiF/Li-Mg). However, after prolonged cycles, LiF/Li-Mg electrode shows much smaller impedances (∼79 Ω) than the Li electrode (∼125 Ω), indicating a reduced side reaction of LiF/Li-Mg electrodes compared to bare Li. Also, we found their stark difference through an air stability test for as-prepared Li and LiF/Li-Mg electrodes exposed to air for 3 h. When we kept the bare Li electrode in an ambient atmosphere

https://doi.org/10.1021/acs.nanolett.3c00764
Nano Lett. 2023, 23, 3582−3591

with a relative humidity (RH) of 25−30%, its silvery color quickly turned to dark gray, and it completely covered the Li surface in 3 h (Figure S10). The bare Li electrode kept in humid air exhibits quite unstable initial Li stripping and increased overpotentials during subsequent cycles. In contrast, the LiF/Li-Mg electrode showed a nearly consistent surface color even after being exposed to air for 3 h (Figure S11). Also, the air-exposed LiF/Li-Mg electrode showed a relatively stable initial cycle and significantly low cell overpotentials compared with the bare Li electrode, indicating that the LiF layer and Li-Mg alloy effectively inhibit the reaction between Li and moisture.

This study highlights the importance of selection of metal fluoride candidates constituting metal elements with Li solubility in designing interface-reinforced Li-M electrodes. As was mentioned before, metal elements with Li solubility (that is, alloying materials with Li) can be largely classified into two groups: one is the solid-solution group (e.g., Mg, Ag, etc.)m and other is the intermetallic compound group (e.g., Sn, Si, Al, In, etc.). When comparing their Li plating/stripping behaviors, the intermetallic compound group is expected to show dramatic XRD peak changes, but the solid-solution group is not. As expected, the as-prepared LiF/Li-Mg electrode shows no XRD peak change, showing a single Li-rich alloy phase even after stripping for 2 h at 1 mA cm^{-2} (with areal capacities of 2 mAh cm^{-2}) (Figure S12). This means that LiF/Li-Mg operates through spontaneous Li diffusion into the Li-Mg alloy phase. On the other hand, it is noteworthy that, in the LiF/Li-Sn electrode, multiphase XRD peaks disappear during cycling, and representative peaks corresponding to crystalline Li are evolved (Figure S13). Because unlike Li-Mg, Li-Sn has discrete reaction potentials above 0.4 V (vs Li^+/Li^0), corresponding to the formation of stoichiometric Li-Sn intermediates,[41] several alloying reactions cannot happen within the operating voltage window (Figure S14). That is why cycled Li in the LiF/Li-Sn electrode could thermodynamically favor deposition on the electrode surface rather than an alloying reaction (or diffusion into the bulk), triggering a relatively low initial CE (ICE) (Figure S15).

In summary, we demonstrate that the evolution of a fluorinated interphase via a conversion-type reaction onto a Li metal surface enables stable Li metal cycling by reducing unwanted side reactions between Li metal and organic electrolytes. Our primary focus is to consider the choice of metal fluorides for interphase evolution based on the phase diagram, particularly whether the metal elements can form an alloy phase with Li or not. Among the different candidates, including FeF_2, CuF_2, SnF_4, and MgF_2, we experimentally showed that metal fluorides composed of Sn and Mg, which react with Li at room temperature, show a satisfactory surface morphology due to their high Li solubility. Particularly, we highlighted that a solid-solution between Li and Mg facilitates a clear separation of the outmost LiF layer from Li-Mg alloy, as well as efficient Li plating/stripping through Li diffusion into the bulk Li-Mg. Our approach offers guidelines for designing the fluorinated interphase evolution and formulating Li alloys for homogeneous Li cycling. Additionally, we propose that additional key parameters affecting relative Li diffusivity within alloys, such as element species, compositions, crystal structures, phase transitions, and crystal defects, should be further investigated to optimize the electrode.

■ ASSOCIATED CONTENT

Supporting Information

The Supporting Information is available free of charge at https://pubs.acs.org/doi/10.1021/acs.nanolett.3c00764.

Materials, experimental procedures, and supporting data (PDF)

In situ TEM movie of the interphase evolution process of MgF_2-anchored nanocapsules (MP4)

■ AUTHOR INFORMATION

Corresponding Author

Hyun-Wook Lee − *School of Energy and Chemical Engineering, Ulsan National Institute of Science and Technology (UNIST), Ulsan 44919, Republic of Korea;* orcid.org/0000-0001-9074-1619; Email: hyunwooklee@unist.ac.kr

Authors

Min-Ho Kim − *School of Energy and Chemical Engineering, Ulsan National Institute of Science and Technology (UNIST), Ulsan 44919, Republic of Korea*

Tae-Ung Wi − *School of Energy and Chemical Engineering, Ulsan National Institute of Science and Technology (UNIST), Ulsan 44919, Republic of Korea; Department of Chemical and Biomolecular Engineering, Rice University, Houston, Texas 77005, United States*

Jeongwoo Seo − *School of Energy and Chemical Engineering, Ulsan National Institute of Science and Technology (UNIST), Ulsan 44919, Republic of Korea*

Ahreum Choi − *School of Energy and Chemical Engineering, Ulsan National Institute of Science and Technology (UNIST), Ulsan 44919, Republic of Korea*

Sangho Ko − *School of Energy and Chemical Engineering, Ulsan National Institute of Science and Technology (UNIST), Ulsan 44919, Republic of Korea*

Juyoung Kim − *School of Energy and Chemical Engineering, Ulsan National Institute of Science and Technology (UNIST), Ulsan 44919, Republic of Korea*

Ukhyun Jung − *School of Energy and Chemical Engineering, Ulsan National Institute of Science and Technology (UNIST), Ulsan 44919, Republic of Korea*

Myeong Seon Kim − *School of Energy and Chemical Engineering, Ulsan National Institute of Science and Technology (UNIST), Ulsan 44919, Republic of Korea*

Changhyun Park − *School of Energy and Chemical Engineering, Ulsan National Institute of Science and Technology (UNIST), Ulsan 44919, Republic of Korea*

Sunghwan Jin − *School of Energy and Chemical Engineering, Ulsan National Institute of Science and Technology (UNIST), Ulsan 44919, Republic of Korea;* orcid.org/0000-0003-3750-8599

Complete contact information is available at: https://pubs.acs.org/10.1021/acs.nanolett.3c00764

Author Contributions

M.-H.K. and H.-W.L. conceived the idea. M.-H.K. carried out the material synthesis, characterization, and electrochemical characterization and wrote the first draft. T.-U.W., S.K., and C.P. conducted cryogenic and *in situ* transmission electron microscope analysis, J.S. and U.J. assisted in sample preparation. All of the authors discussed the experimental

https://doi.org/10.1021/acs.nanolett.3c00764
Nano Lett. 2023, 23, 3582−3591

results and contributed to writing the manuscript. M.-H.K. and T.-U.W. contributed equally to this work.

Notes

The authors declare no competing financial interest.

■ ACKNOWLEDGMENTS

This work was supported by the 2023 Research Fund (1.230040.01) of UNIST and Individual Basic Science & Engineering Research Program (RS-2023-00208929) and the Technology Development Program to Solve Climate Changes (2021M1A2A2038148) through the National Research Foundation (NRF) of Korea funded by the Ministry of Science and ICT (MSIT). S.J. acknowledges support from the NRF grant funded by the MSIT (2021R1C1C2003118). This study contains the results obtained by using the equipment of UNIST Central Research Facilities (UCRF).

■ ABBREVIATIONS

CE	Coulombic efficiency
FEC	Fluoroethylene carbonate
SEI	solid electrolyte interphase
SEM	scanning electron microscopy
XRD	X-ray diffraction
cryo-TEM	cryogenic transmission electron microscopy
NCM811	$Li(Ni_{0.8}Co_{0.1}Mn_{0.1})O_2$
Li-C	lithium-infiltrated carbon composites
LiF/Li-Mg-C	LiF-modified Li-Mg-C composites

■ REFERENCES

(1) Zhang, J.; Xu, W.; Xiao, J.; Cao, X.; Liu, J. Lithium Metal Anodes with Nonaqueous Electrolytes. *Chem. Rev.* **2020**, *120* (24), 13312−13348.

(2) Zheng, G.; Lee, S. W.; Liang, Z.; Lee, H.-W. W.; Yan, K.; Yao, H.; Wang, H.; Li, W.; Chu, S.; Cui, Y. Interconnected Hollow Carbon Nanospheres for Stable Lithium Metal Anodes. *Nat. Nanotechnol.* **2014**, *9* (8), 618−623.

(3) Hobold, G. M.; Lopez, J.; Guo, R.; Minafra, N.; Banerjee, A.; Shirley Meng, Y.; Shao-Horn, Y.; Gallant, B. M. Moving beyond 99.9% Coulombic Efficiency for Lithium Anodes in Liquid Electrolytes. *Nat. Energy* **2021**, *6* (10), 951−960.

(4) Liu, J.; Bao, Z.; Cui, Y.; Dufek, E. J.; Goodenough, J. B.; Khalifah, P.; Li, Q.; Liaw, B. Y.; Liu, P.; Manthiram, A.; Meng, Y. S.; Subramanian, V. R.; Toney, M. F.; Viswanathan, V. V.; Whittingham, M. S.; Xiao, J.; Xu, W.; Yang, J.; Yang, X.-Q.; Zhang, J.-G. Pathways for Practical High-Energy Long-Cycling Lithium Metal Batteries. *Nat. Energy* **2019**, *4* (3), 180−186.

(5) He, X.; Bresser, D.; Passerini, S.; Baakes, F.; Krewer, U.; Lopez, J.; Mallia, C. T.; Shao-Horn, Y.; Cekic-Laskovic, I.; Wiemers-Meyer, S.; Soto, F. A.; Ponce, V.; Seminario, J. M.; Balbuena, P. B.; Jia, H.; Xu, W.; Xu, Y.; Wang, C.; Horstmann, B.; Amine, R.; Su, C.-C.; Shi, J.; Amine, K.; Winter, M.; Latz, A.; Kostecki, R. The Passivity of Lithium Electrodes in Liquid Electrolytes for Secondary Batteries. *Nat. Rev. Mater.* **2021**, *6* (11), 1036−1052.

(6) Fang, C.; Li, J.; Zhang, M.; Zhang, Y.; Yang, F.; Lee, J. Z.; Lee, M.-H.; Alvarado, J.; Schroeder, M. A.; Yang, Y.; Lu, B.; Williams, N.; Ceja, M.; Yang, L.; Cai, M.; Gu, J.; Xu, K.; Wang, X.; Meng, Y. S. Quantifying Inactive Lithium in Lithium Metal Batteries. *Nature* **2019**, *572* (7770), 511−515.

(7) Tikekar, M. D.; Choudhury, S.; Tu, Z.; Archer, L. A. Design Principles for Electrolytes and Interfaces for Stable Lithium-Metal Batteries. *Nat. Energy* **2016**, *1* (9), 16114.

(8) Liang, X.; Pang, Q.; Kochetkov, I. R.; Sempere, M. S.; Huang, H.; Sun, X.; Nazar, L. F. A Facile Surface Chemistry Route to a Stabilized Lithium Metal Anode. *Nat. Energy* **2017**, *2* (July), 1−7.

(9) Moorthy, B.; Kim, J. H.; Lee, H. W.; Kim, D. K. Vertically Aligned Carbon Nanotubular Structure for Guiding Uniform Lithium Deposition via Capillary Pressure as Stable Metallic Lithium Anodes. *Energy Storage Mater.* **2020**, *24*, 602−609.

(10) Tang, W.; Yin, X.; Kang, S.; Chen, Z.; Tian, B.; Teo, S. L.; Wang, X.; Chi, X.; Loh, K. P.; Lee, H.-W.; Zheng, G. W. Lithium Silicide Surface Enrichment: A Solution to Lithium Metal Battery. *Adv. Mater.* **2018**, *30* (34), 1801745.

(11) Kim, M. S.; Zhang, Z.; Rudnicki, P. E.; Yu, Z.; Wang, J.; Wang, H.; Oyakhire, S. T.; Chen, Y.; Kim, S. C.; Zhang, W.; Boyle, D. T.; Kong, X.; Xu, R.; Huang, Z.; Huang, W.; Bent, S. F.; Wang, L.-W.; Qin, J.; Bao, Z.; Cui, Y. Suspension Electrolyte with Modified Li+ Solvation Environment for Lithium Metal Batteries. *Nat. Mater.* **2022**, *21* (4), 445−454.

(12) Chen, S.; Zheng, J.; Mei, D.; Han, K. S.; Engelhard, M. H.; Zhao, W.; Xu, W.; Liu, J.; Zhang, J. High-Voltage Lithium-Metal Batteries Enabled by Localized High-Concentration Electrolytes. *Adv. Mater.* **2018**, *30* (21), 1706102.

(13) Yan, C.; Li, H. R.; Chen, X.; Zhang, X. Q.; Cheng, X. B.; Xu, R.; Huang, J. Q.; Zhang, Q. Regulating the Inner Helmholtz Plane for Stable Solid Electrolyte Interphase on Lithium Metal Anodes. *J. Am. Chem. Soc.* **2019**, *141* (23), 9422−9429.

(14) Ren, X.; Gao, P.; Zou, L.; Jiao, S.; Cao, X.; Zhang, X.; Jia, H.; Engelhard, M. H.; Matthews, B. E.; Wu, H.; Lee, H.; Niu, C.; Wang, C.; Arey, B. W.; Xiao, J.; Liu, J.; Zhang, J. G.; Xu, W. Role of Inner Solvation Sheath within Salt−Solvent Complexes in Tailoring Electrode/Electrolyte Interphases for Lithium Metal Batteries. *Proc. Natl. Acad. Sci. U. S. A.* **2020**, *117* (46), 28603−28613.

(15) Jeon, Y.; Kang, S.; Joo, S. H.; Cho, M.; Park, S. O.; Liu, N.; Kwak, S. K.; Lee, H.-W.; Song, H. Pyridinic-to-Graphitic Conformational Change of Nitrogen in Graphitic Carbon Nitride by Lithium Coordination during Lithium Plating. *Energy Storage Mater.* **2020**, *31* (July), 505−514.

(16) Qian, J.; Henderson, W. A.; Xu, W.; Bhattacharya, P.; Engelhard, M.; Borodin, O.; Zhang, J.-G. High Rate and Stable Cycling of Lithium Metal Anode. *Nat. Commun.* **2015**, *6* (1), 6362.

(17) Wang, J.; Yamada, Y.; Sodeyama, K.; Chiang, C. H.; Tateyama, Y.; Yamada, A. Superconcentrated Electrolytes for a High-Voltage Lithium-Ion Battery. *Nat. Commun.* **2016**, *7* (May), 1−9.

(18) Qiao, L.; Oteo, U.; Martinez-Ibañez, M.; Santiago, A.; Cid, R.; Sanchez-Diez, E.; Lobato, E.; Meabe, L.; Armand, M.; Zhang, H. Stable Non-Corrosive Sulfonimide Salt for 4-V-Class Lithium Metal Batteries. *Nat. Mater.* **2022**, *21* (4), 455−462.

(19) Li, T.; Zhang, X.-Q.; Shi, P.; Zhang, Q. Fluorinated Solid-Electrolyte Interphase in High-Voltage Lithium Metal Batteries. *Joule* **2019**, *3* (11), 2647−2661.

(20) Pathak, R.; Chen, K.; Gurung, A.; Reza, K. M.; Bahrami, B.; Pokharel, J.; Baniya, A.; He, W.; Wu, F.; Zhou, Y.; Xu, K.; Qiao, Q. Q. Fluorinated Hybrid Solid-Electrolyte-Interphase for Dendrite-Free Lithium Deposition. *Nat. Commun.* **2020**, *11* (1), 93.

(21) Kim, S.; Park, S. O.; Lee, M.-Y.; Lee, J.-A.; Kristanto, I.; Lee, T. K.; Hwang, D.; Kim, J.; Wi, T.-U.; Lee, H.-W.; Kwak, S. K.; Choi, N.-S. Stable Electrode−Electrolyte Interfaces Constructed by Fluorine- and Nitrogen-Donating Ionic Additives for High-Performance Lithium Metal Batteries. *Energy Storage Mater.* **2022**, *45*, 1−13.

(22) Zhang, X. Q.; Cheng, X. B.; Chen, X.; Yan, C.; Zhang, Q. Fluoroethylene Carbonate Additives to Render Uniform Li Deposits in Lithium Metal Batteries. *Adv. Funct. Mater.* **2017**, *27* (10), 1605989.

(23) Suo, L.; Xue, W.; Gobet, M.; Greenbaum, S. G.; Wang, C.; Chen, Y.; Yang, W.; Li, Y.; Li, J. Fluorine-Donating Electrolytes Enable Highly Reversible 5-V-Class Li Metal Batteries. *Proc. Natl. Acad. Sci. U. S. A.* **2018**, *115* (6), 1156−1161.

(24) Li, Y.; Li, Y.; Pei, A.; Yan, K.; Sun, Y.; Wu, C.; Joubert, L.-M.; Chin, R.; Koh, A. L.; Yu, Y.; Perrino, J.; Butz, B.; Chu, S.; Cui, Y. Atomic Structure of Sensitive Battery Materials and Interfaces Revealed by Cryo−Electron Microscopy. *Science (80-.)* **2017**, *358* (6362), 506−510.

(25) Zhang, Z.; Li, Y.; Xu, R.; Zhou, W.; Li, Y.; Oyakhire, S. T.; Wu, Y.; et al. Capturing the Swelling of Solid-Electrolyte Interphase in Lithium Metal Batteries. *Science (80-.)* **2022**, *375* (6576), 66−70.

https://doi.org/10.1021/acs.nanolett.3c00764
Nano Lett. 2023, 23, 3582−3591

(26) Wang, X.; Li, Y.; Meng, Y. S. Cryogenic Electron Microscopy for Characterizing and Diagnosing Batteries. *Joule* **2018**, *2* (11), 2225−2234.
(27) Wang, T.; Duan, J.; Zhang, B.; Luo, W.; Ji, X.; Xu, H.; Huang, Y.; Huang, L.; Song, Z.; Wen, J.; Wang, C.; Huang, Y.; Goodenough, J. B. A Self-Regulated Gradient Interphase for Dendrite-Free Solid-State Li Batteries. *Energy Environ. Sci.* **2022**, *15* (3), 1325−1333.
(28) Li, F.; Tan, Y.-H.; Yin, Y.-C.; Zhang, T.-W.; Lu, L.-L.; Song, Y.-H.; Tian, T.; Shen, B.; Zhu, Z.-X.; Yao, H.-B. A Fluorinated Alloy-Type Interfacial Layer Enabled by Metal Fluoride Nanoparticle Modification for Stabilizing Li Metal Anodes. *Chem. Sci.* **2019**, *10* (42), 9735−9739.
(29) Sun, Y.; Lee, H. W.; Zheng, G.; Seh, Z. W.; Sun, J.; Li, Y.; Cui, Y. In Situ Chemical Synthesis of Lithium Fluoride/Metal Nanocomposite for High Capacity Prelithiation of Cathodes. *Nano Lett.* **2016**, *16* (2), 1497−1501.
(30) Qian, J.; Adams, B. D.; Zheng, J.; Xu, W.; Henderson, W. A.; Wang, J.; Bowden, M. E.; Xu, S.; Hu, J.; Zhang, J. G. Anode-Free Rechargeable Lithium Metal Batteries. *Adv. Funct. Mater.* **2016**, *26* (39), 7094−7102.
(31) Wan, M.; Kang, S.; Wang, L.; Lee, H. W.; Zheng, G. W.; Cui, Y.; Sun, Y. Mechanical Rolling Formation of Interpenetrated Lithium Metal/Lithium Tin Alloy Foil for Ultrahigh-Rate Battery Anode. *Nat. Commun.* **2020**, *11* (1), 1−10.
(32) Zhao, Q.; Stalin, S.; Archer, L. A. Stabilizing Metal Battery Anodes through the Design of Solid Electrolyte Interphases. *Joule* **2021**, *5* (5), 1119−1142.
(33) Li, H.; Yamaguchi, T.; Matsumoto, S.; Hoshikawa, H.; Kumagai, T.; Okamoto, N. L.; Ichitsubo, T. Circumventing Huge Volume Strain in Alloy Anodes of Lithium Batteries. *Nat. Commun.* **2020**, *11* (1), 1584.
(34) Zhang, S.; Yang, G.; Liu, Z.; Weng, S.; Li, X.; Wang, X.; Gao, Y.; Wang, Z.; Chen, L. Phase Diagram Determined Lithium Plating/Stripping Behaviors on Lithiophilic Substrates. *ACS Energy Lett.* **2021**, *6* (11), 4118−4126.
(35) Krauskopf, T.; Mogwitz, B.; Rosenbach, C.; Zeier, W. G.; Janek, J. Diffusion Limitation of Lithium Metal and Li−Mg Alloy Anodes on LLZO Type Solid Electrolytes as a Function of Temperature and Pressure. *Adv. Energy Mater.* **2019**, *9* (44), 1902568.
(36) Zhang, Y.; Chandran, K. S. R.; Jagannathan, M.; Bilheux, H. Z.; Bilheux, J. C. The Nature of Electrochemical Delithiation of Li-Mg Alloy Electrodes: Neutron Computed Tomography and Analytical Modeling of Li Diffusion and Delithiation Phenomenon. *J. Electrochem. Soc.* **2017**, *164* (2), A28−A38.
(37) Kong, L.; Wang, L.; Ni, Z.; Liu, S.; Li, G.; Gao, X. Lithium−Magnesium Alloy as a Stable Anode for Lithium−Sulfur Battery. *Adv. Funct. Mater.* **2019**, *29* (13), 1808756.
(38) Nandiyanto, A. B. D.; Iskandar, F.; Ogi, T.; Okuyama, K. Nanometer to Submicrometer Magnesium Fluoride Particles with Controllable Morphology. *Langmuir* **2010**, *26* (14), 12260−12266.
(39) Xiao, A. W.; Lee, H. J.; Capone, I.; Robertson, A.; Wi, T.; Fawdon, J.; Wheeler, S.; Lee, H.; Grobert, N.; Pasta, M. Understanding the Conversion Mechanism and Performance of Monodisperse FeF2 Nanocrystal Cathodes. *Nat. Mater.* **2020**, *19*, 644.
(40) Go, W.; Kim, M. H.; Park, J.; Lim, C. H.; Joo, S. H.; Kim, Y.; Lee, H. W. Nanocrevasse-Rich Carbon Fibers for Stable Lithium and Sodium Metal Anodes. *Nano Lett.* **2019**, *19* (3), 1504−1511.
(41) Park, C.-M.; Kim, J.-H.; Kim, H.; Sohn, H.-J. Li-Alloy Based Anode Materials for Li Secondary Batteries. *Chem. Soc. Rev.* **2010**, *39* (8), 3115.

https://doi.org/10.1021/acs.nanolett.3c00764
Nano Lett. 2023, 23, 3582−3591